Catalysis Letters 23 (1994) 251–262

Strong modification of Pt–CO interaction caused by alloying with chromium in Pt–Cr/HZSM-5 catalysts

Olga P. Tkachenko, Efim S. Shpiro

N.D. Zelinsky Institute of Organic Chemistry, Russian Academy of Sciences, 47 Leninsky Prospect, 117913 Moscow, Russia

Nils I. Jaeger, Ryszard Lamber, Günter Schulz-Ekloff and Holger Landmesser

Institut für Angewandte und Physikalischer Chemie, Universität Bremen, FB2-Biologie/Chemie, D-2800 Bremen 33, Germany

Received 19 May 1993; accepted 20 September 1993

The catalysts Pt/HZSM-5 and Pt–Cr/HZSM-5 are characterized by FTIR spectroscopy using CO as a probe molecule, and by transmission electron microscopy. The major fraction of the metal phase detected in the micrographs exhibits particles in the range of 1–3 nm uniformly distributed in the zeolite crystals. Nanodiffraction analysis of single particles confirmed the formation of fcc Pt–Cr alloy with lattice constant $a = 0.386$ nm. The infrared spectra at 300 K exhibit bands assigned to CO linearly bonded to zeolite-hosted metal particles at 2089 cm^{-1} for Pt/HZSM-5, and at 2120 and 2092 cm^{-1} for Pt–Cr/HZSM-5. The temperature increase to 610 K resulted in a strong shift of the 2089 cm^{-1} band for Pt/HZSM-5 by 25 cm^{-1} and a slight shift of the corresponding bands for Pt–Cr/HZSM-5 by 6 cm^{-1}. The differences are referred to different electron backdonation capacities of the CO binding Pt surface atoms of the metal particles. The lower capacity for the Pt–Cr/HZSM-5 sample is due to alloying in the metal particles.

Keywords: Pt–Cr alloy; ZSM-5; CO adsorption; FTIR; HRTEM; nanodiffraction

1. Introduction

Platinum based bimetallic catalysts are of considerable importance for the petrochemical industry [1]. The optimization of these catalysts is closely related to the elucidation of promoting effects produced by additive metals. A general structural model was proposed in an attempt to explain promoting effects in platinum-based catalysts [2]. According to this model the top surface layer of an alloy particle consists entirely of platinum while the second layer is enriched in the additive metal. Experimental evidence for Pt monolayer segregation was obtained for Pt–Cr/HZSM-5 catalysts [3,4]. Platinum was found by LEISS to be strongly enriched on

the surface of the Pt–Cr alloy and the hydrogenolysis activity of the Pt–Cr/HZSM-5 was found to be much lower compared to that of the monometallic Pt/HZSM-5 catalyst.

The nature of the modification of platinum by alloying with chromium and its relevance with respect to adsorption and catalysis, however, is not yet well understood. Numerous IR studies of CO adsorption on supported Pt catalysts showed that stretching frequency and relative intensity of CO bands are sensitive to the oxidation state [5,7], particle size [6,8–13], metal–support interaction [10,13,14] and alloying [15–17]. The effect of platinum alloying by Pb, Cu, Sn, Re on IR CO bands was discussed by Ponec et al. [15–17]. The largest of the observed downward shifts (30–50 cm^{-1}) was found for Pt–Pb alloy on Al_2O_3 and was attributed to an increase of $d \rightarrow \pi^*$ backdonation. A correlation between enthalpy of alloy formation and CO band shift could not be established [16]. Remarkable differences in mono- and bimetallic samples were found earlier in an EXAFS/XANES/XPS study [3,4,18] and ascribed to Pt–Cr alloying.

This paper presents FTIR data on CO adsorption and the temperature dependence of spectra for both Pt/HZSM-5, and Pt–Cr/HZSM-5. The metal particle sizes are determined using transmission electron microscopy.

2. Experimental

Sample preparation. The samples studied were 0.5% Pt/HZSM-5 and 0.5% Pt–0.75% Cr/HZSM-5 prepared by impregnation of HZSM-5 (Si/Al = 18) with aqueous solution of platinum(II)-tetrammine dichloride and simultaneous impregnation with both H_2PtCl_6 and CrO_3 solution according to the procedure described earlier [3,4,18]. The samples were calcined in air and then reduced in flowing hydrogen at 790 K.

FTIR measurements. The Fourier transform infrared spectra were recorded on a BIO-RAD single beam FTIR spectrometer in the range of 400–4000 cm^{-1} with a resolution of 2 cm^{-1}. The specimens were pressed into thin wafers and mounted in a cell connected to a turbomolecular pump and to a gas handling system [19]. Before spectra recording the samples were evacuated and again reduced in flowing hydrogen of 10^{-3} Pa at 610 K. After pretreatment background spectra were recorded in the absence of CO at different temperatures. The sample was then exposed to flowing CO at 10^{-3} Pa for 15 min. In a first series of runs the CO flow was admitted at 300 K and IR spectra were measured in the presence of the gas phase. Then the cell was evacuated and spectra were taken at 300 K and during heating up at 423, 473, 573 and 608–615 K, respectively. In a second series, samples were continuously treated with flowing CO and the spectra were recorded at the same set of temperatures. In all cases IR spectra were corrected by corresponding background spectra.

Transmission electron microscopy. TEM was carried out with a Philips EM 420

T electron microscope (LaB_6 filament) operated at 120 kV and equipped with an energy dispersive X-ray analyzer (EDX). The catalysts were ground to a fine powder, deposited on a copper grid coated with a carbon film and dispersed on the grid ultrasonically. No organic solvents were used during this procedure. Details of the technique are reported in ref. [20]. The elemental composition of the metal particles was checked by using EDX with a stationary TEM probe. A large number of individual metal particles have been analyzed in the nanoprobe mode with a spot size of about 10–12 nm. Smaller probe sizes led to counting rates too low due to the low current in the electron probe. Information regarding the structure of the metal particles was derived from nanodiffraction patterns, which could be obtained by using a small (5 nm) stationary electron probe.

3. Results

3.1. TRANSMISSION ELECTRON MICROSCOPY OF Pt/HZSM-5 AND Pt–Cr/HZSM-5

A transmission electron micrograph of the Pt/HZSM-5 specimen is shown in fig. 1a. Platinum is present in the form of small particles with sizes in the range between 1 and 3 nm located within the zeolite matrix. These results are consistent with earlier data obtained by XPS, EXAFS and TEM [3,21] showing preferential location of platinum inside the zeolite structure possibly in channel intersections and some voids. Unlike to data reported in ref. [21] a minor fraction of large aggregates (6–10 nm) can also be detected outside the zeolite crystals. The formation of a few big particles can be attributed to a more rapid temperature increase during sample calcination.

A typical micrograph of the Pt–Cr/HZSM-5 sample is shown in fig. 1b. Metallic particles in the range between 1 and 3 nm are visible, which is consistent with earlier data [3,4]. EDX spectra obtained when the electron probe was focussed on a single particle showed the signals both for Pt and Cr which is indicative of a bimetallic particle.

The comparison of the Pt and Cr peak heights obtained for different metal crystallites indicates some differences in composition.

EDX analysis of particle free areas on the specimen showed weak Cr signals possibly due to unreduced chromium ions. To estimate possible differences in the structure of metallic particles nanodiffraction analysis of about 40 individual particles was performed. It gives lattice constant values which could be divided into two groups $a_1 = 0.384–0.388$ nm and $a_2 = 0.389–0.392$ nm. Normally, for these broad reflexes in nanodiffraction the absolute error could be estimated as ± 0.005 nm. The distance between two values, however, can be ascertained with a standard deviation of only ± 0.002 nm. About 60% of the crystallites have an average lattice constant $a = 0.386$ whereas about 40% showed a lattice parameter $a = 0.391$ nm, which is close to that of bulk platinum ($a_{Pt} = 0.392$ nm). Fig. 2 shows an example of

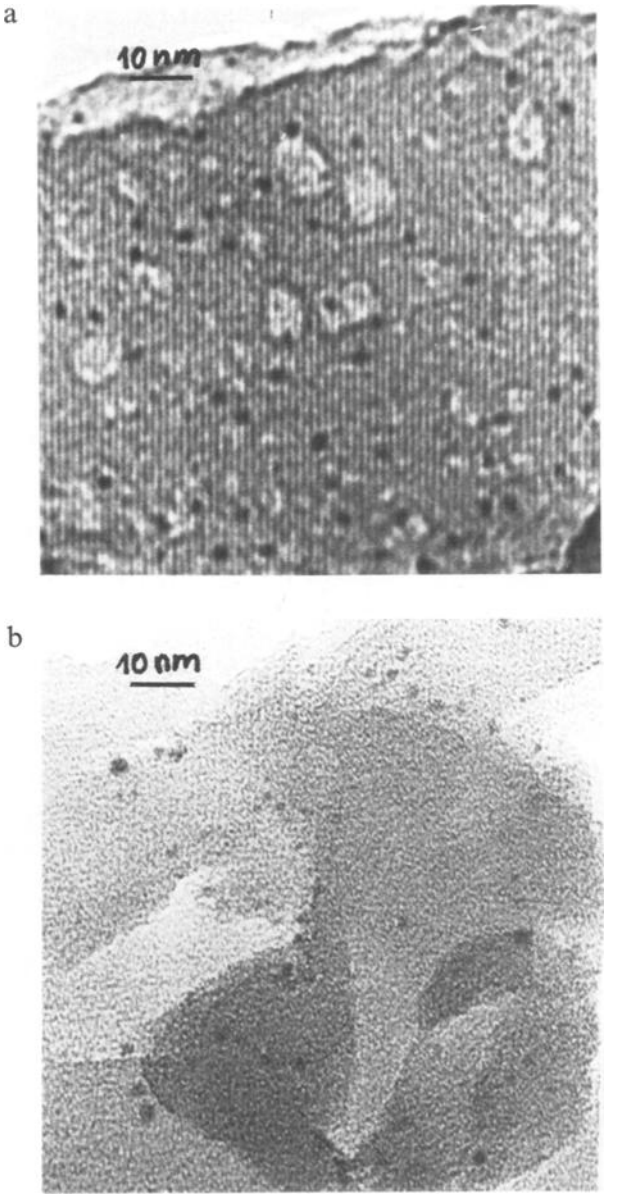

Fig. 1. (a) Electron micrograph of the Pt/HZSM-5 specimen. The (101) lattice fringes (1.1 nm) of the zeolite matrix are visible. (b) Electron micrographs of the Pt–Cr/HZSM-5 sample. Both pictures are on the same scales.

a nanodiffractogram which can be ascribed to a fcc crystallite ($a = 0.386$ nm) in the [112] orientation. The appearance of metal crystallites with the fcc structure and a lattice parameter $a = 0.391$ nm can be explained by the presence of Pt crystallites in the Pt–Cr/HZSM-5 sample.

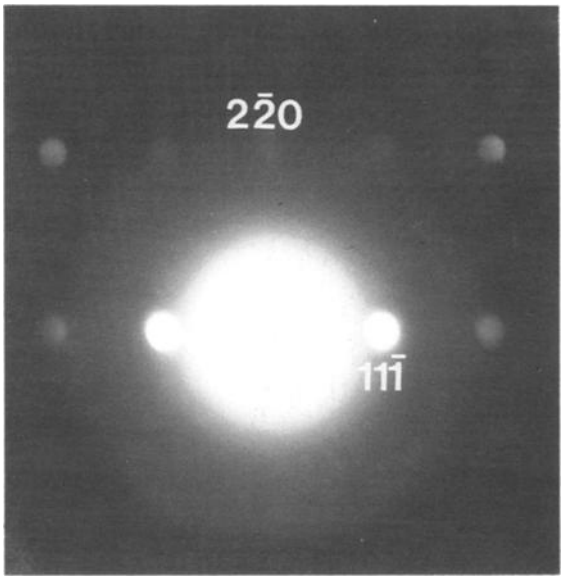

Fig. 2. Nanodiffraction pattern obtained from a particle with the fcc structure ($a = 0.386$ nm) in the [112] orientation.

Metal aggregates with an average lattice constant $a = 0.386$ nm can be understood in terms of the formation of a Pt–Cr solid solution, which was reported to crystallize in the fcc structure [22]. Using data on changes of the Pt lattice parameter induced by the incorporation of chromium [22], it is estimated that the atomic concentration of the chromium is about 30–40%. It should be noted that very diluted Pt–Cr alloy particles (less than 15%) could not be distinguished from pure Pt particles due to the rather large error in the determination of the lattice constant.

3.2. FTIR SPECTROSCOPY

3.2.1. Pt/HZSM-5

CO adsorption at room temperature over Pt/HZSM-5 reduced at 790 K leads to the appearance of the spectra typical for metallic Pt with a strong and narrow band at 2089 cm^{-1} (high frequency band (HFB)) assigned to linearly bonded CO (fig. 3a). A weak signal of bridge bonded CO at 1887 cm^{-1} ([5,7,8,14], table 1) can also be seen for this sample. Evacuation results in a small shift of the principal band to 2087 cm^{-1} (fig. 4a). The temperature dependence of the band position demonstrates a downward shift during the temperature increase from 300 to 473 K by 23 cm^{-1}. A second CO adsorption at 300 K essentially reproduced the spectra

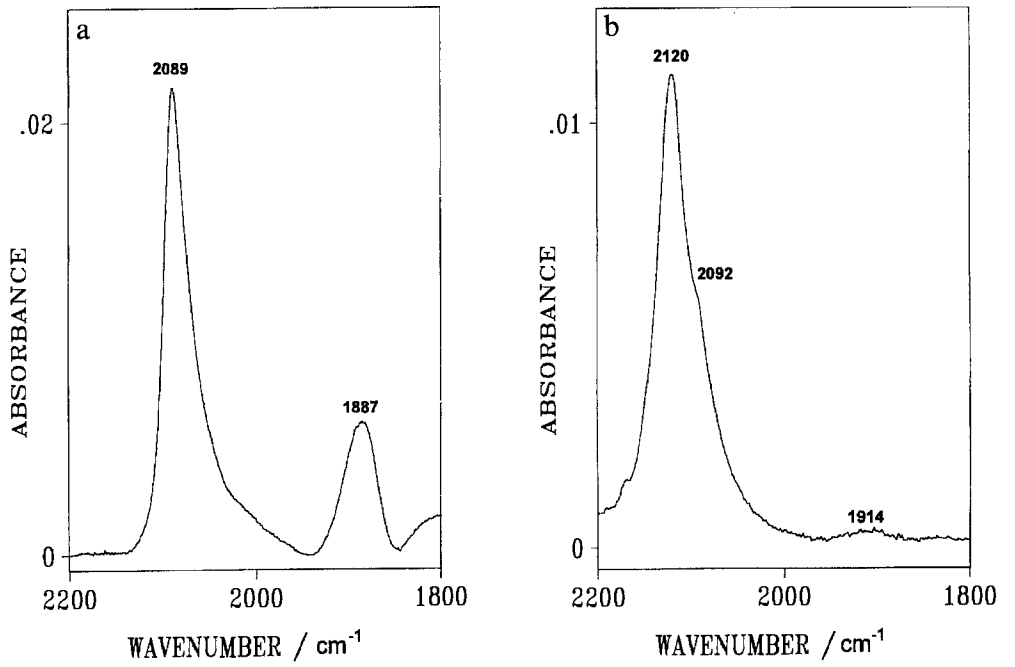

Fig. 3. FTIR spectra of CO adsorbed at 300 K on: Pt/HZSM-5 (a) and Pt–Cr/HZSM-5 (b); in flowing CO (10 Pa).

shown in fig. 4a. The other feature observed when CO is adsorbed on Pt/HZSM-5 is the difference in thermostability of CO adsorbed in vacuum or in flowing CO. In the first case the CO band vanished beyond 573 K (fig. 4a). In flowing CO (10^{-3} Pa) the adsorption can be observed up to 600 K (fig. 4b).

3.2.2. Pt–Cr/HZSM-5

CO adsorption at 300 K results in the appearance of a strong and poorly resolved doublet at 2120 cm^{-1} (main peak, very high frequency band (VHFB)) and 2092 cm^{-1} (shoulder, high frequency band (HFB)) along with a band of 1914 cm^{-1} (fig. 3b). After CO evacuation the doublet became more resolved. The weak band initially located at 2172 cm^{-1} was no longer observed. Further evacuation during temperature increase does not change noticeably the resolution of the components (fig. 5a). Both, the VHFB and the HFB are shifted only very slightly by 5 cm^{-1} during the temperature increase from 300 to 610 K, i.e. the temperature dependence of these bands is quite different from that observed on Pt/HZSM-5. Unlike in the case of platinum, CO adsorbed at 300 K remains on the surface during desorption in vacuum (fig. 5a) as well as in flowing CO (fig. 5b) up to 610 K. The band at 1914 cm^{-1} observed at 300 K is believed to be due to bridge bonded CO. The weak band could not be related to the possible influence of an alloy.

Table 1
Assignment of wavenumbers of CO adsorbed on platinum

Catalyst	Wavenumber (cm^{-1})	Assignment	Ref.
Pt/HZSM-5	2089–2064	Pt–CO	this work
	1887	bridge bonded	
Pt–Cr/HZSM-5	2120–2114	$Pt^{\delta+}$–CO	this work
	2092–2088	Pt–CO	
Pt/NaX	2180–2200	Pt^{2+}–CO	[27]
	2130–2150	(PtO)–CO	
	2100–2120	$Pt^{\delta+}$–CO	
	2100, 2035	$(O_Z)_2Pt(CO)_2$	
Pt/NaY	2076–2049	Pt–CO	[14]
Pt/HNaY	2082–2060	Pt–CO	
6.2% Pt/Al_2O_3	2123	$Pt^{\delta+}$–CO	[5]
	2092	(CO)Pt(O)	
	2073	Pt–CO	
	1850	bridge bonded	
0.6% Pt/Al_2O_3	2152–2133	Pt^{n+}–CO	[7]
	2081	Pt–CO	
	1900	bridge bonded	
	1850	bridge bonded	
Pt/Al_2O_3	2080–2052	Pt–CO (depending on	[10]
	(θ = 1–0.1)	coverage)	
	2120	O(Pt)–CO	
0.3% Pt/SiO_2	2070	Pt–CO	[13]
0.3% Pt/Al_2O_3	2060	Pt–CO	
Pt(111)	2101–2065	Pt–CO	[23]

4. Discussion

The frequency at 2089–2087 cm^{-1} can be assigned to linearly bonded CO on Pt/HZSM-5 (figs. 3a and 4a). It is within the range observed for Pt/Al_2O_3, Pt/SiO_2, remarkably higher as compared to Pt/NaY ([5,8,13,14], table 1) and rather close to those observed for Pt particles in PtHNaY zeolite [14]. The higher frequency is not related to a size effect but rather to metal–support interaction. Indeed, Pt particles of similar size in NaY zeolite exhibit bands in the range of 2049–2076 cm^{-1} ([14], table 1) which is lower than for Pt(111) single crystal surfaces ([23], table 1). There are two possible reasons for the higher frequency band (HFB) observed with Pt/HZSM-5, i.e. (1) dipole–dipole coupling of adsorbed

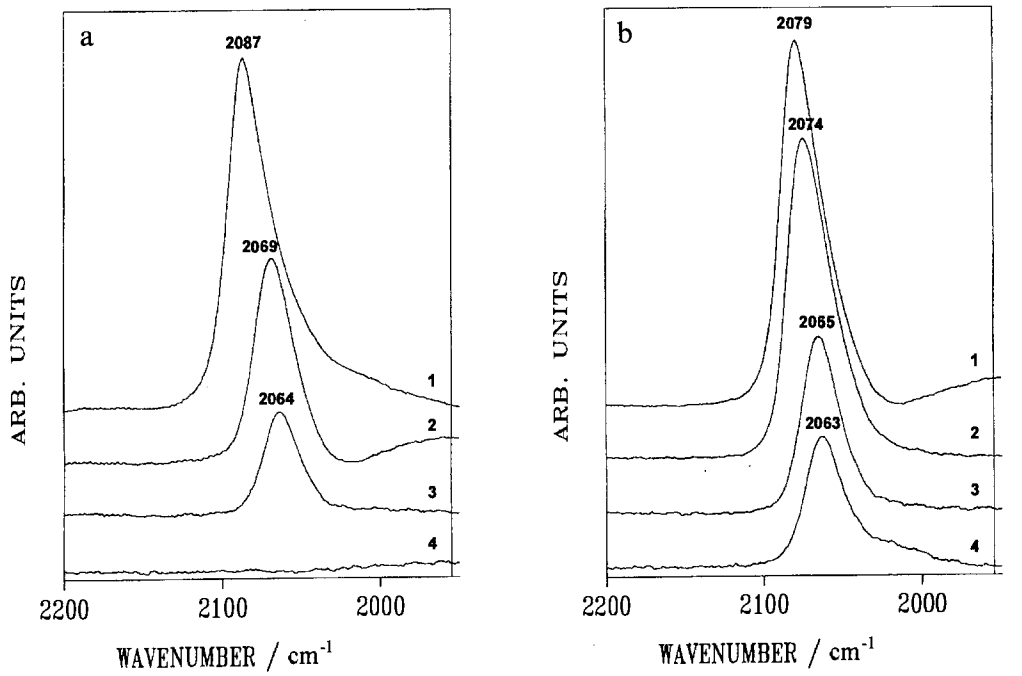

Fig. 4. FTIR spectra of CO adsorbed on Pt/HZSM-5: (a) CO evacuation during heating from 300 K (1) up to 423 K (2), 473 K (3) and 573 K (4); (b) CO adsorption at different temperatures: 423 K (1), 473 K (2), 573 K (3) and 600 K (4).

molecules and/or (2) electron deficiency of metallic particles in HZSM-5 zeolite. The temperature dependence of the band position (fig. 4a) which undergoes a downward shift of about 23 cm^{-1} indeed indicates a lateral interaction in the adsorbate layer at the higher coverage present at room temperature [10]. On the other hand, the frequency of 2064 cm^{-1} at low coverages is still higher than observed for Pt supported on NaY [14], which might be due to platinum–acidic proton interaction. Similar metal–zeolite support interactions were observed for Pd_n microclusters in PdHNaY zeolite [24]. The decrease of the HFS during heating in CO (fig. 4b) might be attributed to a decrease of this metal–zeolite support interaction.

An interpretation of the CO stretching vibration for the bimetallic Pt–Cr/HZSM-5 sample is not so straightforward as for monometallic Pt/HZSM-5. The CO adsorption on chromium sites may contribute to the spectra. Adsorption on Cr^0 should lead to low frequency bands in the range of 1820–2000 cm^{-1} which are not observed. Adsorption on Cr cationic sites (Cr^{3+} or Cr^{2+}) gives bands in the range of 2130–2250 cm^{-1} [25,26]. That means, only the weak band at 2172 cm^{-1} (fig. 3b) can be ascribed to CO adsorption on Cr cations. Thus, we can rule out that the most intense line at 2113–2120 cm^{-1} reflects an adsorption on Cr centers. On the other hand this band was often observed on supported Pt catalysts and was ascribed to incompletely reduced Pt ([5,27], table 1). However, the existence of Pt^{2+}

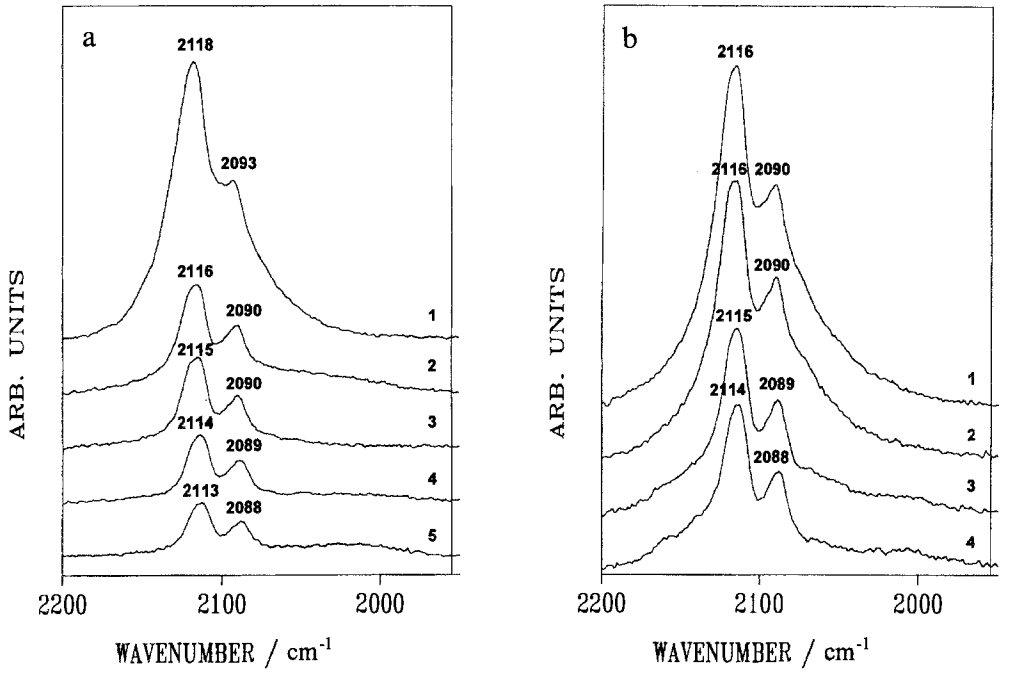

Fig. 5. FTIR spectra of CO adsorbed on Pt–Cr/HZSM-5: (a) CO evacuation during heating from 300 K (1) up to 423 K (2), 473 K (3), 573 K (4) and 610 K (5); (b) CO adsorption at different temperatures: 423 K (1), 473 K (2), 573 K (3) and 610 K (4).

cations which give bands at 2185–2200 cm^{-1} [27] can also be excluded. Other cationic species such as Pt^+ or Pt/PtO could give rise to CO bands around and above 2100 cm^{-1} ([5,7,10,27], table 1). However, the results obtained earlier [3,18,21] and now indicate rather clearly that such species are not predominant in the Pt–Cr sample reduced at 793 K. While in a precalcined Pt–Cr catalyst cationic Pt species were easily detected by XPS they were no longer observed after hydrogen reduction [3]. HRTEM and EXAFS showed the formation of small metallic particles in both Pt/ZSM-5 and Pt–Cr/ZSM-5, the fcc structure was evaluated from the analysis of four nearest neighbour Pt–Pt shells in Pt L EXAFS [3,21]. These particles are coordinated by zeolitic framework oxygen but the Pt–O bond contribution is small and equal for both samples. Moreover, no Pt–O bond length typical for PtO_x species could be detected. The influence of the metal–zeolite support interaction on the Pt–Pt bond was equal for both Pt/HZSM-5 and Pt–Cr/HZSM-5 zeolites [3,18]. A dicarbonyl $Pt(CO)_2$ which might form in the presence of Pt^+ or Pt/PtO species gives two bands [27] but with distinctly different separation (2100 cm^{-1} (asym.) and 2030 cm^{-1} (sym.)) and cannot be the origin of the observed bands in figs. 5a and 5b. It can therefore be concluded that the VHFB belongs to a $Pt^{\delta+}$ species in a Pt–Cr alloy.

The results obtained by nanodiffraction analysis of single particles (fig. 2) gave

clear evidence for the existence of alloyed Pt/Cr-metal particles in Pt–Cr/HZSM-5 which agrees well with previous EXAFS data [18]. In addition a part of the Pt particles is not alloyed or contains very little chromium. The TEM results (figs. 1a, 1b) show that size distribution and morphology of the small particles cannot be distinguished. The interpretation of the FTIR spectra therefore does not consider differences in morphology. Moreover, an increase of sites with lower coordination number for smaller Pt–Cr particles should result in a decrease of the CO frequency [11]. In agreement with these results and FTIR spectra obtained for Pt/HZSM-5 (fig. 5a) the VHF band at 2118 cm^{-1} can be ascribed to CO adsorbed on the Pt–Cr alloy while the additional band at 2088–2093 cm^{-1} (figs. 5a and 5b) can most likely be assigned to CO bonded to Pt particles.

It must be noted, however, that the strong shift of this band observed in the temperature program for Pt/HZSM-5 (fig. 4) was not observed in this case.

The generation of $Pt^{\delta+}$ species at the surface of a Pt–Cr alloy can be related to the structural peculiarity of the alloy particles, i.e., the segregation in the surface domain resulting in a layer of platinum atoms at the surface and a layer of chromium atoms in the subsurface [2–4]. The formation of $Pt^{\delta+}$ sites is related to the interaction between surface Pt atoms and subsurface Cr atoms, which could be in a zerovalent or in a higher oxidation state. CO adsorption at $Pt^{\delta+}$ atoms results in a reduced backdonation capability from the metal d-orbitals to the antibonding π^*-orbitals of the CO molecule. Consequently, the vibration of the CO bond is shifted to higher frequency, thus, explaining the VHFB. Obviously, the CO molecules adsorbed at the layer of $Pt^{\delta+}$ atoms have a lower tendency for lateral interactions as can be concluded from the small shift of only 6 cm^{-1} of the VHFB with varying coverage in the temperature range of 300–615 K.

A reduced backdonation capability of Pt–Cr alloy particles was also assumed as a reason for the suppression of C–C bond cleavage in hydrocarbon conversion on Pt–Cr/HZSM-5 catalysts [4]. The postulated charge transfer from noble metal surface layers to subsurface layers of alloying transition metals is supported by recent XPS results [28]. Corresponding effects are observed for Pt–Co and Pt–Ti alloys, and are also explained by the surface segregation model [29,30]. The reason for deviating observations [15–17] is not clear, and could be due to differences of the valency state of the electropositive metal in the subsurface layer.

The origin of the HFB of the doublet might be due to CO adsorption (1) on Pt particles in the Pt–Cr/HZSM-5 catalyst which do not contain Cr or (2) on Pt atoms which do not exhibit a marked electron deficiency due to a low Cr content in the alloy.

5. Conclusions

(1) The electron micrographs demonstrate that small metal particles are formed

both in Pt/HZSM-5 and Pt–Cr/HZSM-5 catalysts while EDX and nanodiffraction analysis clearly show Pt–Cr alloy formation in the latter sample.

(2) The FTIR spectra of CO on Pt/HZSM-5 catalysts show a high frequency band at 2089 cm^{-1} related to CO adsorption at electron deficient Pt clusters inside the highly acidic zeolite matrix.

(3) The FTIR spectra of CO on Pt–Cr/HZSM-5 catalysts exhibit a very high frequency band at 2120 cm^{-1} assigned to an adsorption at Pt–Cr alloy particles indicating additional electron deficiency of surface platinum atoms in an alloy.

Acknowledgement

Financial support by the Deutsche Forschungsgemeinschaft (AZ 438 113-139) and by the BMFT (03C 258 3) is gratefully acknowledged.

References

[1] J.H. Sinfelt, in: *Catalysis: Science and Technology*, Vol. 1, eds. J.R. Anderson and M. Boudart (Springer, Berlin, 1981) p. 257.
[2] R.W. Joyner and E.S. Shpiro, Catal. Lett. 9 (1991) 239.
[3] R.W. Joyner, E.S. Shpiro, P. Johnston and G.G. Tuleuova, Part I, J. Catal. (1993), in press.
[4] R.W. Joyner, E.S. Shpiro, P. Johnston and G.G. Tuleuova, Part II, J. Catal. (1993), in press.
[5] Y. Barshad, X. Zhou and E. Gulari, J. Catal. 94 (1985) 128.
[6] H. Bischoff, N.I. Jaeger and G. Schulz-Ekloff, Z. Phys. Chem. (Leipzig) 271 (1990) 1093.
[7] L. Marchese, M.R. Boccuti, S. Coluccia, S. Lavagnino, A. Zecchina, L. Bonneviot and M. Che, in: *Structure and Reactivity of Surfaces*, Stud. Surf. Sci. Catal., Vol. 48, eds. C. Morterra, A. Zecchina and G. Costa (Elsevier, Amsterdam, 1989) p. 653.
[8] R. Barth, R. Pitchai, R.L. Anderson and X.E. Verykios, J. Catal. 116 (1989) 61.
[9] C. Besoukhanova, J. Guidot, D. Barthomeuf, M. Breysse and J.R. Bernard, J. Chem. Soc. Faraday Trans. I 77 (1981) 1595.
[10] M. Primet, L.-C. de Menorval, J. Fraissard and T. Ito, J. Catal. 88 (1984) 273.
[11] M.J. Kappers and J.H. van der Maas, Catal. Lett. 10 (1991) 365.
[12] A.A. Solomennikov, Y.A. Lokhov, A.A. Davidov and A.Y. Ryndin, Kinet. Katal. 20 (1979) 589.
[13] R. Barth and A. Ramachandran, J. Catal. 125 (1990) 467.
[14] A. de Mallmann and D. Barthomeuf, in: *Zeolites as Catalysts, Sorbents and Detergent Builders*, Stud. Surf. Sci. Catal., Vol. 46, eds. H.G. Karge and J. Weitkamp (Elsevier, Amsterdam, 1989) p. 429.
[15] F.J.C.M. Toolenaar, F. Stoop and V. Ponec, J. Catal. 82 (1983) 1.
[16] A.G.T.M. Bastein, F.J.C.M. Toolenaar and V. Ponec, J. Catal. 90 (1984) 88.
[17] H.A.C.M. Hendrickx and V. Ponec, Surf. Sci. 192 (1987) 234.
[18] R.W. Joyner, Kh.M. Minachev, P.D.A. Pudney, E.S. Shpiro and G.G. Tuleuova, Catal. Lett. 5 (1990) 257.
[19] H. Bischoff, N.I. Jaeger and G. Schulz-Ekloff, Catal. Today 8 (1991) 501.
[20] R. Lamber, N.I. Jaeger, A. Trunschke and H. Miessner, Catal. Lett. 11 (1991) 1.
[21] E.S. Shpiro, R.W. Joyner, Kh.M. Minachev and P.D. Pudney, J. Catal. 127 (1991) 366.

[22] W. Bronger and W. Klemm, Z. Anorg. Allg. Chem. 319 (1962) 58.
[23] P. Hollins, Surf. Sci. Rep. 16 (1992) 51.
[24] J.L. Sheu, H. Knözinger and W.M.H. Sachtler, J. Mol. Catal. 57 (1989) 61.
[25] A. Zecchina, E. Garrone, G. Ghiotti, C. Morterra and E. Borello, J. Phys. Chem. 79 (1975) 966, 972, 978.
[26] B. Rebenstorff, Z. Anorg. Allg. Chem. 571 (1989) 148.
[27] H. Bischoff, N.I. Jaeger, G. Schulz-Ekloff and L. Kubelkova, J. Mol. Catal. 80 (1993) 95, and references therein.
[28] R.A. Cambell, J.A. Rodriguez and D.W. Goodman, *Proc. 10th Int. Congr. on Catalysis*, Budapest 1992, eds. L. Guczi, F. Solymosi and P. Tétényi (Akadémia Kiado, Budapest, 1993) p. 36.
[29] J. Paul, S.D. Cameron, D.J. Dwyer and F.M. Hoffmann, Surf. Sci. 177 (1986) 121.
[30] U. Bardi, B.C. Beard and P.N. Ross, J. Catal. 124 (1990) 22.